Spectroscopic Peculiarities at Ionization of Excited $2p^5(^2P_{J_f})3s[K]_{0,1,2}$ States of Ne: Cooper Minima and Autoionizing Resonances

Maria M. Popova [1,2] , **Maksim D. Kiselev** [1,2,3] , **Sergei M. Burkov** [4] , **Elena V. Gryzlova** [2,*] and **Alexei N. Grum-Grzhimailo** [2,3]

[1] Faculty of Physics, Lomonosov Moscow State University, 119991 Moscow, Russia
[2] Skobeltsyn Institute of Nuclear Physics, Lomonosov Moscow State University, 119991 Moscow, Russia
[3] School of Physics and Engineering, ITMO University, 197101 Saint Petersburg, Russia
[4] Laboratory for Modeling of Quantum Processes, Pacific National University, 680035 Khabarovsk, Russia
[*] Correspondence: gryzlovaev@depni.sinp.msu.ru; Tel.: +7-905-763-2237

Abstract: An extensive study of photoionization from neon excited states was performed. The R-matrix approach was applied to calculate a photoionization cross-section from the metastable $2p^5(^2P_{J_f})3s[K]_{0,2}$ and dipole-allowed $2p^5(^2P_{J_f})3s[K]_1$ states. The resonance structures and Cooper minimum accessible in photoionization from the excited states by the photons with energy below 30 eV were analyzed. The parameters of the lowest autoionizing states (AISs) of even parity were extracted by fitting of the photoionization cross-section. For the dipole-allowed states, calculations are presented for unpolarized, linearly and circularly polarized radiation.

1. Introduction

The investigations of photoprocesses from excited states being particularly interesting for studies in non-linear optics, plasma physics and the interpretation of astrophysical data from planet and stellar atmospheres [1] are suppressed by the fact that their relaxation may occur faster than photoionization. Up to recently, there were two frameworks overcoming this obstacle: measuring photoionization of metastable states and pump-probe experiments. Both schemes are restricted in terms of states they may be applied to. The first one because only the lowest atomic states are metastable, and the second one because at least one of the pump-probe fields should be intense, and therefore is supposed to be in the optic region. The extensive review of both the experimental and theoretical research devoted to ionization from excited states is presented in [2]. With the advent of Free Electron Laser facilities (FEL), the available set of states has extended enormously. Due to such sources of high-intensity radiation, the photoionization of excited states can be studied in two-photon resonance ionization.

It was M.Ya. Amusia [3] who pointed out that, opposite to common expectations that with the increase of a shell quantum number photoionization cross-sections would tend to become hydrogen-like, ionization from an excited state may manifest even more characteristic features: "The deviations of many-electron atoms from hydrogen-like ones are still essential even for comparatively high values of the ionised level's quantum number n for any frequencies in the vicinity of the threshold and far away from it".

In particular, Cooper minimum [4,5] may appear even in the $l \rightarrow l-1$ channel [6] in photoionization cross-sections from excited states, in contrast to the photoionization from ground states [7,8]. The Cooper minimum is one of the most famous among characteristic

features, which can be explained in terms of single-electron amplitudes, but its position, form and depth are very sensitive to electron–electron correlations.

Electron–electron correlations are known to be of a great importance for the explanation of characteristic features in photoionization [9–14]. They provide a very severe and challenging test for theoretical models. Nowadays, the characteristic features of noble gases have attracted a lot of attention in connection with time-delay studies [15–18].

Another important characteristic feature of a continuum is autoionizing states [19,20]. In the noble gases, odd-parity AISs with $J = 1$ can be photoexcited from the ground state and have been investigated in great detail [21–24]. AISs with $J \neq 1$, including the AISs of even parity, are populated in multiphoton processes, probably involving discrete excited states [25–27]. A multistep or multiphoton excitation allows reaching a state of any parity and angular momentum, but Cooper minima in this process has another nature [28,29]. From this point of view, the photoionization of prepared or pumped states provides different pieces of information about atomic continuum.

In noble gases, even the lowest discrete states ($\sim$10 eV) may be excited only by VUV radiation. The setup based on the joined action of synchrotron radiation and optic (IR) laser (pump-probe scheme) has been widely used for investigations of the photoionization of excited states to the near-threshold region, including the Rydberg AIS [30–33]. The ionization of the metastable states of noble gases populated by glow discharge method (optogalvanic spectroscopy) or by electron or ion impact [34] also has been a subject of numerous investigations [35–42]. To describe characteristic features in the photoionization of noble gases from excited states (Cooper minima and Rydberg AIS), different methods were applied: quantum defect theory [43], R-matrix [44], configuration interaction Pauli–Fock with a core polarization method [31,41,45] and MCHF [46].

While the Rydberg AIS of the $np^5(^2P_{1/2})ml$ configuration can be reached via VUV + IR two-photon transition, even-parity AIS with the hole-particle or doubly excited configurations can be reached only via two-photon (resonantly enhanced) ionization by VUV radiation [47–50]. Before FEL development, these AISs were investigated basically by electron- or ion-impact method [51–53].

Since intense photon pulses were obtained with the advent of FELs, and resonance few-photon ionization of atoms and ions of noble gases was observed [54–57], the problem of obtaining accurate two-photon cross-sections and cross-sections from the excited states in the XUV region has arisen.

Here, we present an extensive study of neon photoionization from excited states. The lowest excited states are metastable $2s^22p^5(^2P_{J_f})3s[K]_{0,2}$ (here and after core $1s^2$ is omitted for brevity) and the states which can be reached from the ground by dipole excitation (dipole-allowed) $2s^22p^5(^2P_{J_f})3s[K]_1$. We use the intermediate jK-coupling scheme, where a core angular momentum J_f is coupled with an electron orbital momentum l to quantum number K, and then intermediate momentum K and electron spin $1/2$ are coupled to total angular momentum J of a system. The cross-sections are obtained by the B-spline R-matrix approach in realization by O.I. Zatsarinny [58,59]. This approach provided a high quality of oscillator strength for neon ground state excitations [60] and excellent agreement for the ionization of potassium excited states [61].

The paper is organized as follows: in Section 2, we present the results obtained within different models for metastable $2s^22p^5(^2P_{J_f})3s[K]_{0,2}$ states and compare the models with each other and with available experimental data; in Section 3, we present the results obtained in a few models chosen based on Section 2 and calculated for different field polarizations for dipole-allowed $2s^22p^5(^2P_{J_f})3s[K]_1$ states; and in Section 4, we discuss the parameters of autoionizing structures.

2. PhotoIonization of Metastable $2s^22p^5(^2P_{1/2})3s[1/2]_0$ and $2s^22p^5(^2P_{3/2})3s[3/2]_2$ States

The B-spline R-matrix (BSR) approach [58] allows the orbitals of initial and target states, as well as different target states, to be non-orthogonal. With this advantage, wave functions of the initial (excited atomic) and target (ionic) states can be obtained in series of

independent MCHF calculations [62]. The approach allows to account for the dependence of the individual one-electron orbitals on states of interest and accurately describe them, keeping configuration expansions compact. The R-matrix approach automatically accounts for electron correlations in the continuum, leading to essential channel interactions.

In a pure jK-coupling scheme, the allowed ionization channels are:

$$2s^2 2p^5 (^2P_{1/2}) 3s [1/2]_0 + \gamma \rightarrow 2s^2 2p^5 (^2P_{1/2}) + \varepsilon p \quad J = 1 ; \tag{1}$$
$$2s^2 2p^5 (^2P_{3/2}) 3s [3/2]_2 + \gamma \rightarrow 2s^2 2p^5 (^2P_{3/2}) + \varepsilon p \quad J = 1 , 2 , 3 ; \tag{2}$$

but due to channel interactions, the weaker channels, including εf-wave, emerge:

$$2s^2 2p^5 (^2P_{1/2}) 3s [1/2]_0 + \gamma \rightarrow 2s^2 2p^5 (^2P_{3/2}) + \varepsilon p / \varepsilon f \quad J = 1 ; \tag{3}$$
$$2s^2 2p^5 (^2P_{3/2}) 3s [3/2]_2 + \gamma \rightarrow 2s^2 2p^5 (^2P_{1/2}) + \varepsilon p / \varepsilon f \quad J = 1 , 2 , 3 . \tag{4}$$

We explore three models with the subsequent Breit–Pauli diagonalization procedure [63] to take into account spin–orbit interaction: the model based on using real orthogonal orbitals (addressed as $\mathcal{R}$-model), the model with the use of non-orthogonal virtual orbitals ($\mathcal{V}$-model) and the approach combining both real and virtual orbitals ($\mathcal{C}$-model). For all of them, different numbers of target ionic states (see Table 1) are considered in the B-spline, bound-state close-coupling calculations. The number of accounted target states was varied: two ($2s^2 2p^5$ ($^2P_{3/2,1/2}$)) — to include direct photoionization only; six (+ $2s 2p^6$ ($^2S_{1/2}$) and $2s^2 2p^4 3s$ ($^4P_{5/2,3/2,1/2}$)) — to allow generation of the lowest AISs, either hole-particle or doubly excited; ten (+ $2s^2 2p^4 3s$ ($^2P_{3/2,1/2}$) and $2s^2 2p^4 3s$ ($^2D_{5/2,3/2}$)); and thirteen (+ $2s^2 2p^4 3p$ ($^4P_{5/2,3/2,1/2}$)) — to shift the AIS energies closer to their experimental positions [53,64].

Table 1. Target states (named by the leading term in LSJ approximation), the leading terms in configuration mixing (in percent) and energies according to NIST database [65]. Core $1s^2$ is omitted for brevity.

Target	Energy	$\mathcal{R}$-Model	$\mathcal{V}$-Model	$\mathcal{C}$-Model
$2s^2 2p^5$ ($^2P_{3/2}$)	21.5645	99.92 $2s^2 2p^5$+0.03 $2s^2 2p^4 3p$+	92.80 $2s^2 2p^5$+3.16 $2s^2 2p^4 3\bar{p}$+	98.24 $2s^2 2p^5$+0.56 $2s^2 2p^3 4\bar{p}^2$+
$2s^2 2p^5$ ($^2P_{1/2}$)	21.6613	0.02 $2s^2 2p^3 3p^2$+0.01 $2s^2 2p^4 4p$	2.70 $2s 2p^5 3\bar{s}$+0.36 0.37 $2s^2 2p^3 3\bar{p}^2$	0.54 $2s^2 2p^3 3\bar{d}^2$+0.35 $2s 2p^5 3\bar{d}$
$2s 2p^6$ ($^2S_{1/2}$)	48.4750	95.39 $2s 2p^6$+4.03 $2s^2 2p^4 3s$+	93.58 $2s 2p^6$+2.26 $2s^2 2p^4 3\bar{d}$+	94.70 $2s 2p^6$+2.33 $2s^2 2p^4 3\bar{d}$+
		0.23 $2s p^5 3p$+0.21 $2s^2 2p^4 4s$	0.77 $2s^2 2p^4 3\bar{d}^2$+0.67 $2s^2 2p^4 3s$	0.79 $2s^2 2p^4 3\bar{d}^2$+0.75 $2s^2 2p^4 4\bar{p}^2$
$2s^2 2p^4 3s$ ($^4P_{5/2}$)	48.7333	95.13 $2s^2 2p^4 3s$+3.76 $2s^2 2p^4 4s$	97.28 $2s^2 2p^4 3s$+1.24 $2s^2 2p^4 3s^2$+	91.68 $2s^2 2p^4 3s$+4.98 $2s^2 2p^4 4\bar{s}$
$2s^2 2p^4 3s$ ($^4P_{3/2}$)	48.7975	0.79 $2s^2 2p^3 3s 3p$+0.10 $2s 2p^5 3p$	0.58 $2s^2 2p^4 3s 3\bar{d}$+0.35 $2s^2 2p^3 3s 3\bar{p}^2$	0.66 $2s^2 2p^3 3s 4\bar{p}$+0.62 $2s^2 2p^4 3s 3\bar{d}$
$2s^2 2p^4 3s$ ($^4P_{1/2}$)	48.8345	91.80 $2s^2 2p^4 3s$+3.63 $2s^2 2p^4 4s$		
		3.48 $2s 2p^6$+0.76 $2s^2 2p^3 3s 3p$		
$2s^2 2p^4 3s$ ($^2P_{3/2}$)	49.3478	95.40 $2s^2 2p^4 3s$+3.41 $2s^2 2p^4 4s$+	97.70 $2s^2 2p^4 3s$+0.72 $2s^2 2p^4 3s^2$+	94.02 $2s^2 2p^4 3s$+2.50 $2s^2 2p^4 4\bar{s}$+
$2s^2 2p^4 3s$ ($^2P_{1/2}$)	49.4237	1.38 $2s^2 2p^3 3s 4p$+0.84 $2s^2 2p^3 3s 3p$	0.59 $2s^2 2p^4 3s 3\bar{d}$+0.35 $2s^2 2p^3 3s 3\bar{p}^2$	1.38 $2s^2 2p^3 3s 4\bar{p}$+0.74 $2s^2 2p^3 3s 3p$
$2s^2 2p^4 3p$ ($^4P_{5/2}$)	52.0885	94.37 $2s^2 2p^4 3p$+4.70 $2s^2 2p^4 4p$+	90.78 $2s^2 2p^4 3p$+6.67 $2s^2 2p^3 3p 4\bar{p}$+	96.73 $2s^2 2p^4 3p$+1.67 $2s^2 2p^3 3p 4\bar{p}$+
$2s^2 2p^4 3p$ ($^4P_{3/2}$)	52.1161	0.55 $2s^2 2p^3 3p^2$+0.14 $2s^2 2p^3 3p 4p$	1.77 $2s^2 2p^4 3p 3\bar{s}$+0.48 $2s 2p^4 3p 3\bar{d}$	0.58 $2s^2 2p^4 3p 3\bar{d}$+0.49 $2s^2 2p^3 3p^2$
$2s^2 2p^4 3p$ ($^4P_{1/2}$)	52.1388			
$2s^2 2p^4 3s$ ($^2D_{5/2}$)	52.1135	95.30 $2s^2 2p^4 3s$+3.71 $2s^2 2p^4 4s$+	97.38 $2s^2 2p^4 3s$+1.01 $2s^2 2p^4 3s^2$+	92.77 $2s^2 2p^4 3s$+4.03 $2s^2 2p^4 4\bar{s}$+
$2s^2 2p^4 3s$ ($^2D_{3/2}$)	52.1139	0.73 $2s^2 2p^3 3s 3p$+0.16 $2s^2 2p^3 3s 4p$	0.62 $2s^2 2p^4 3s 3\bar{d}$+0.38 $2s^2 2p^3 3s 3\bar{d}^2$	1.16 $2s^2 2p^3 3s 4\bar{p}$+0.66 $2s^2 2p^4 3s 3\bar{d}$

For the interpolation procedure, we use B-splines of the 8th order. The R-matrix radius is chosen to be 80 a.u. Moreover, we fix grid parameters: $h = 0.0125$ a.u. (step size at the origin, from 0 to 1) and $h_{max} = 0.5$ a.u. (maximum step size of the grid). These parameters were chosen in such a way that for all of the models the resulting accuracy is enough to correctly reproduce the radial part of the wave functions.

The models have the same set of configuration state functions (CSFs), including the ones with excited core to account the core–valence correlations. The initial $2s^2 2p^5 (^2P_{J_f}) 3s [K]_{0,1,2}$ states' CSFs include all possible single and double replacements of $2s$, $2p$ and $3s$ orbitals with $n = 3, 4 ; l = s, p, d, f$-orbitals; and target states' CSFs include single and double replacements of $2s$, $2p$ and $3s$ orbitals to each of the orbitals $n = 3, 4 ; l = s, p, d, f$ solely. For example, in the $2s 2p^6 (^2S_{1/2})$ decomposition, there are $2s 2p^4 3p^2$ and $2s 2p^4 4p^2$ configu-

rations, but there is no $2s2p^43p4p$. In the calculation, we use the energies of target states adjusted to the experimental values [65].

In the $\mathcal{R}$-model, the initial and target states are obtained using the same real orbitals: the first set of $1s$, $2s$ and $2p$ orbitals is optimized on the $2s^22p^5$ configuration and frozen for forthcoming calculations, then each of the real $3s$–$4f$ orbitals is optimized on the corresponding configuration with the highest weights in the CSFs set of $2s^22p^5(^2P_{3/2})3s[3/2]_1$ state, i.e., $3s$, $4s$, $3d$ and $4d$ orbitals are optimized on $2s^22p^5nl$ configuration and $3p$, $4p$ and $4f$ orbitals on $2s^22p^43snl$. The main contributions to both metastable $2s^22p^5(^2P_{J_f})3s[K]_{0,2}$ states came from

$$2s^22p^53s(99.81\%)\,,2s^22p^54s(0.07\%)\,,2s^22p^43s3p(0.05\%)\,,2s^22p^33s3p^2(0.03\%)\,,2s^22p^53d(0.02\%)$$

configurations. The main contributions to the target states are presented in Table 1.

In the $\mathcal{V}$-model, the CSFs of the initial and target states are optimized independently. Thereof, the orbitals of the leading configuration ($1s$, $2s$ and $2p$) are real; orbitals $3d - 4f$ are correlation pseudo-orbitals, and $3s$ and $3p$ orbitals may be real or virtual depending on the state of interest. All orbitals were allowed to vary together. The main contributions to both $2s^22p^5(^2P_{J_f})3s[K]_{0,2}$ states came from

$$2s^22p^53s(93.09\%)\,,2s^22p^43s3p(2.86\%)\,,2s2p^53s4s(2.45\%)\,,2s2p^33s3p^2(0.42\%)\,,2s2p^33s3d(0.37\%)$$

configurations. The main contributions to the target states are presented in Table 1. The difference between theoretical and experimental target energies in this model is less than 0.1 eV.

In the $\mathcal{C}$-model, we keep all of the orbitals presented in target states leading configurations ($1s - 3p$) as they are obtained in the $\mathcal{R}$-model; therefore, they are real and orthogonal. The other ($3d - 4f$) pseudo-orbitals are optimized separately for different targets and non-orthogonal. The initial states are the same as in the $\mathcal{R}$-model. The main contributions to the target states are presented in Table 1.

In Figures 1 and 2, cross-sections of photoionization from $2s^22p^5(P_{1/2})3s[1/2]_0$ and $2s^22p^5(P_{3/2})3s[3/2]_2$ metastable states are presented for these three models, with different numbers of target states in length and velocity gauges. The upper row (a,b,c) in Figure 1 and bottom row (d,e,f) in Figure 2 present results for photoionization which is forbidden within the pure jK-coupling scheme, the bottom row in Figure 1 and upper row in Figure 2 for allowed. In the featureless region (from 3 to 20 eV), cross-sections for allowed ionization are higher than for forbidden one.

The cross-section of allowed photoionization manifests the Cooper minimum near the threshold; the one of the forbidden photoionization does not. The energy of Cooper minimum is basically determined by the nodes of $3s$-orbital. That is the reason why cross-sections in $\mathcal{R}$- and $\mathcal{C}$-models based on the same $3s$-orbitals are alike at low energies. The Cooper minimum is more pronounced in the $\mathcal{V}$-model because the wave function of the initial state is more compact when virtual orbitals are included. The more target states are included, the farther Cooper minimum is pushed below the ionization threshold. A further analysis has shown that for larger CSF sets of target states, the Cooper minimum is pushed less. With the exception of the model with the fewest (two) number of target states, Cooper minima are deeper and situated at a little higher energy for calculations in the length gauge.
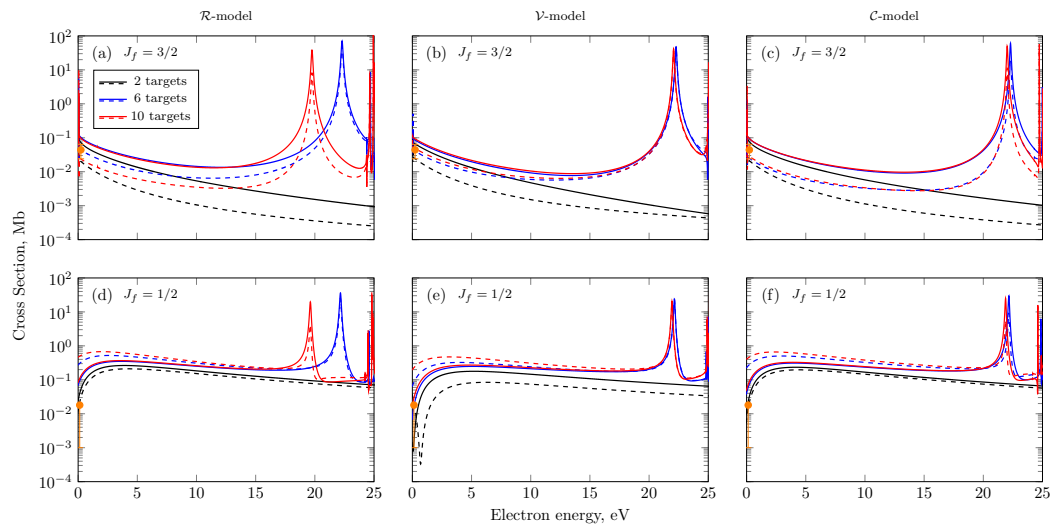
Figure 1. Photoionization cross-section of $2s^22p^5(P_{1/2})3s[1/2]_0$ state of neon to $2s^22p^5\,(^2P_{3/2})$ (upper row) and $2s^22p^5\,(^2P_{1/2})$ (bottom row). Calculations are performed within $\mathcal{R}$- (**a**,**d**), $\mathcal{V}$- (**b**,**e**) and $\mathcal{C}$-model (**c**,**f**). Solid lines are for calculations in the length gauge and dashed lines in the velocity gauge; different colors mark the number of accounted target states: two (black), six (blue) and ten (red). Experimental data points are taken from [38] and labeled by orange.
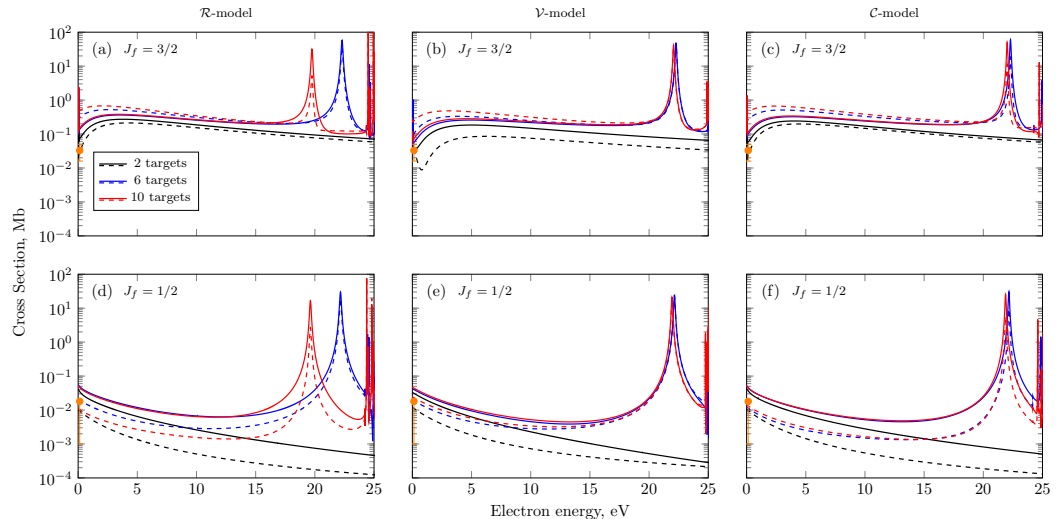

Figure 2. Photoionization cross-section of $2s^22p^5(^2P_{3/2})3s[3/2]_2$ state of neon to $2s^22p^5\,(^2P_{3/2})$ (upper row) and $2s^22p^5\,(^2P_{1/2})$ (bottom row). Calculations are performed within $\mathcal{R}$- (**a**,**d**), $\mathcal{V}$- (**b**,**e**) and $\mathcal{C}$-model (**c**,**f**). Solid lines are for calculations in the length gauge and dashed for the velocity gauge; different colors mark the number of accounted targets: two (black), six (blue) and ten (red). Experimental data points are taken from [38] and labeled by orange.

The resonance structure at ∼22 eV is hole-particle $2s2p^63s\,(^3S_1)$ AIS generated on the $2s2p^6\,(^2S)$ target; inclusion of the other targets may shift the position of the structure. Their influence depends on how close a target energy is to the ^2S-target. Note that only states with total momentum $J = 1$ can be excited from the $2s^22p^5(^2P_{1/2})3s[1/2]_0$ metastable state. The position of the AIS weakly depends on the model and is in accordance with that reported in [53], except for the $\mathcal{R}$-model, where the enabling of $2s^22p^43s\,(^2D_{5/2,3/2})$ target states leads to a dramatic jump in the resonance energy position (Figures 1a and 2a, red curves). In the $\mathcal{V}$- and $\mathcal{C}$-models, these ^2D targets slightly (by 0.3 eV) move the resonance position down towards the experimental value. In the $\mathcal{R}$-model, it is impossible to match the energy position of $2s2p^6\,(^2S_{1/2})$ and $2s^22p^43s\,(^2D_{5/2,3/2})$ target states, and interference

between them is more essential than it is supposed to be in reality. The parameters of the resonance are discussed in Section 4.

As was pointed out in [60], introducing virtual orbitals is necessary to obtain good agreement between length and velocity gauges, and in the considered case, overall agreement is better for the $\mathcal{V}$-model, especially for the forbidden photoionization. We checked that the addition of $5\bar{l}(\bar{l}=\bar{s},\bar{p},\bar{d},\bar{f})$ orbitals to the expansion of $2s^2 2p^5(^2P_{J_f})3s[K]_{0,2}$ states in $\mathcal{R}$- and $\mathcal{C}$-models makes the cross-sections look similar to the ones obtained within the $\mathcal{V}$-model (not shown) and pulls the Cooper minimum above the threshold. Nevertheless, it is important to notice that while the $\mathcal{V}$-model provides much faster convergence than the $\mathcal{R}$- and $\mathcal{C}$-models, the last two reproduce near-threshold behavior of angular anisotropy parameter β for the forbidden photoionization much better. Among the models with virtual orbitals, the ones including only $2s2p^5 n\bar{l}^2$-type (with $n=3,4$; $l=s,p,d,f$) pair-excitations additionally to $2s^2 2p^5 n\bar{s}+2s^2 2p^5 n\bar{d}$ ($n=3,4$) single-excitations provide an angular anisotropy parameter similar to the one in [38] and hit the experimental values. The models allowing contributions of single excitations to $3p,4p,4f$ fail because configuration $2s^2 2p^4 3s3\bar{p}$ obtains the highest weight after $2s^2 2p^5 3s$. However, in the cross-sections, the difference between the use of the two sets of orbitals described above is hardly seen.

The issue is very similar to that recorded for electron scattering involving $2p^5 3s$ states: while there are models reproducing angle-integrated data [66], additional actions are needed to reproduce differential parameters [67].

3. Photoionization of Dipole-Allowed $2s^2 2p^5(^2P_{J_f})3s[K]_1$ States

In this section, we present calculations of photoionization cross-sections from dipole-allowed $2s^2 2p^5(^2P_{J_f})3s[K]_1$ states, which can be effectively excited by an electromagnetic field. To the best of our knowledge, there are very few updated data for them in the literature [47,50,68]. This data may be useful for the interpretation of experiments involving two-photon (probably two-color) processes at FELs [54–56]. One of the advantages of modern FELs and synchrotron facilities is that the generated radiation is polarized. Bearing in mind this possibility, we present here calculations for three cases: both exciting and ionizing fields are unpolarized, linearly polarized in the same direction and circularly polarized with equal helicities. Accounting for the dipole selection rules, the cross-section for unpolarized radiation is $\sigma^{(u)}=s_0(|D_{J=0}|^2+|D_{J=1}|^2+|D_{J=2}|^2)/3$, for linearly polarized $\sigma^{(l)}=s_0(|D_{J=0}|^2/3+2|D_{J=2}|^2/15)$ and for circularly polarized $\sigma^{(c)}=s_0|D_{J=2}|^2/5$ [46,69], where $s_0=4\pi\omega/3c$ and D_J is the reduced dipole matrix transition amplitude. The cross-sections by unpolarized and polarized radiation do not share spectroscopic features because different channels are involved.

In Figures 3 and 4, we present results for photoionization of $2s^2 2p^5(^2P_{3/2})3s[3/2]_1$ and $2s^2 2p^5(^2P_{1/2})3s[1/2]_1$ states, correspondingly calculated within the $\mathcal{V}$- and $\mathcal{C}$-models accounting for six and ten target states. The upper row (a,b,c) in Figure 3 and bottom row (d,e,f) in Figure 4 present allowed photoionization.

$$2s^2 2p^5(^2P_{1/2})3s[1/2]_1 + \gamma \;\rightarrow\; 2s^2 2p^5(^2P_{1/2}) + \varepsilon l \quad J = 0,1,2\,; \tag{5}$$

$$2s^2 2p^5(^2P_{3/2})3s[3/2]_1 + \gamma \;\rightarrow\; 2s^2 2p^5(^2P_{3/2}) + \varepsilon l \quad J = 0,1,2\,; \tag{6}$$
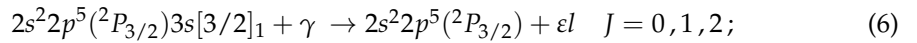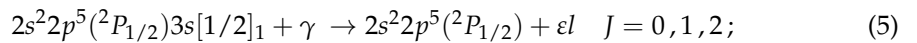
The bottom row (d,e,f) in Figure 3 and upper row (a,b,c) in Figure 4 present forbidden photoionization:

$$2s^2 2p^5(^2P_{1/2})3s[1/2]_1 + \gamma \;\rightarrow\; 2s^2 2p^5(^2P_{3/2}) + \varepsilon l/\varepsilon f \quad J = 0,1,2\,; \tag{7}$$

$$2s^2 2p^5(^2P_{3/2})3s[3/2]_1 + \gamma \;\rightarrow\; 2s^2 2p^5(^2P_{1/2}) + \varepsilon l/\varepsilon f \quad J = 0,1,2\,. \tag{8}$$
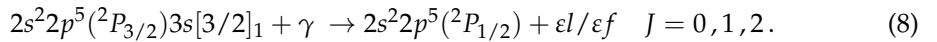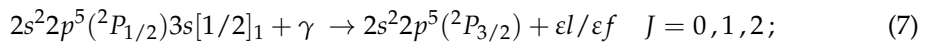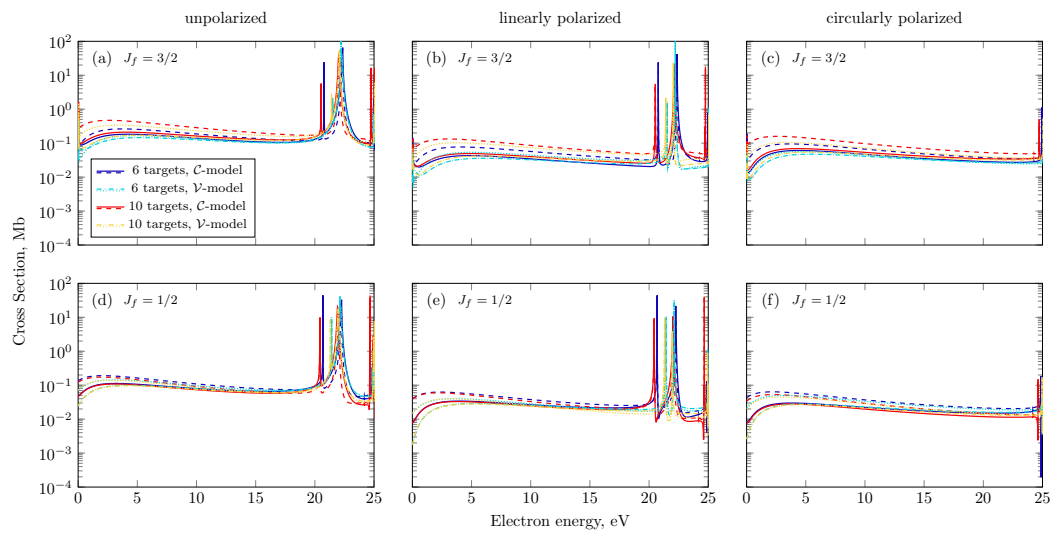
Figure 3. Cross-section calculated within the $\mathcal{V}$- (dash-dotted lines correspond to length gauge, dotted lines to velocity gauge) and $\mathcal{C}$- (solid lines correspond to length gauge, dashed lines to velocity gauge) models with six (cyan and blue) and ten (orange and red) target states for ionization of $2s^2 2p^5 (^2P_{3/2}) 3s[3/2]_1$ state to $2s^2 2p^5 (^2P_{3/2})$ (upper row) and $2s^2 2p^5 (^2P_{1/2})$ (bottom row) ionic states for unpolarized (**a,d**), linearly polarized (**b,e**) and circularly polarized (**c,f**) fields.
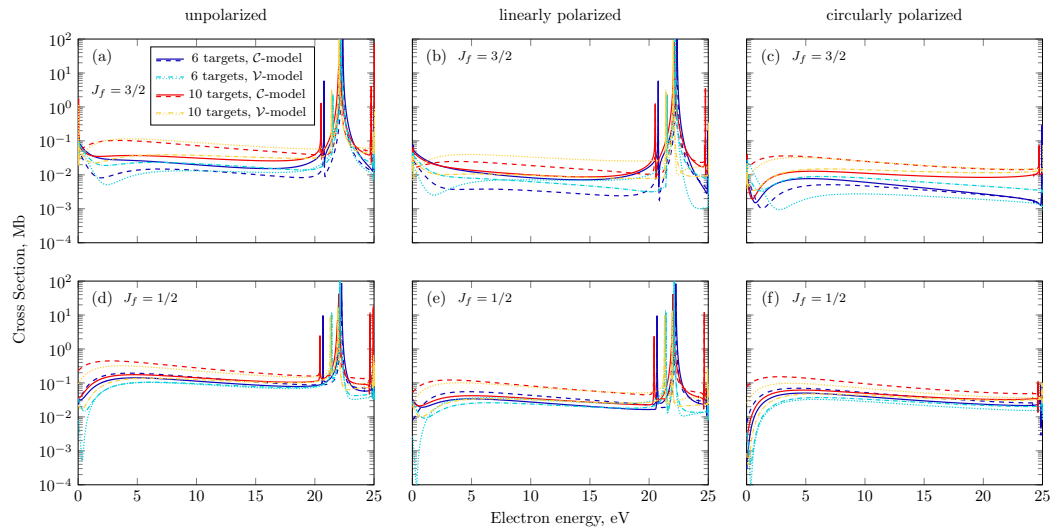

Figure 4. Cross-section calculated within the $\mathcal{V}$- (dash-dotted lines correspond to length gauge, dotted lines to velocity gauge) and $\mathcal{C}$- (solid lines correspond to length gauge, dashed lines to velocity gauge) models with six (cyan and blue) and ten (orange and red) target states for ionization of $2s^2 2p^5 (^2P_{1/2}) 3s[1/2]_1$ state to $2s^2 2p^5 (^2P_{3/2})$ (upper row) and $2s^2 2p^5 (^2P_{1/2})$ (bottom row) ionic states for unpolarized (**a,d**), linearly polarized (**b,e**) and circularly polarized (**c,f**) fields. Within the $\mathcal{V}$-model, orange and cyan lines in panels (**d,e,f**) practically coincide.

Notice that in the smooth region, "allowed" and "forbidden" photoionization does not differ that much as for the metastable states, because these states are not pure, neither in the jK-scheme, nor in the LS one: in the $\mathcal{C}$-model $2s^2 2p^5 (^2P_{1/2}) 3s[1/2]_1 = 0.89\, 2s^2 2p^5 3s\,^1P - 0.45\, 2s^2 2p^5 3s\,^3P + \ldots$ and in the $\mathcal{V}$-model $2s^2 2p^5 (^2P_{1/2}) 3s[1/2]_1 = 0.89\, 2s^2 2p^5 3s\,^1P - 0.38\, 2s^2 2p^5 3s\,^3P + \ldots$, which differs from the pure jK-scheme where the coefficients are $2s^2 2p^5 (^2P_{1/2}) 3s[1/2]_1 = 0.82\, 2s^2 2p^5 3s\,^1P - 0.58\, 2s^2 2p^5 3s\,^3P$.

For the allowed photoionization, the manifestation of the Cooper minimum strongly depends on polarization; in the case of circular polarization where only channels with $J = 2$ can contribute, it is placed very close to the threshold (Figures 3c and 4f). In the case of linear polarization, additional allowed channels with $J = 0$ shift the Cooper minimum to

higher energy (Figures 3b and 4e). Finally, the channels with $J = 1$ allowed for unpolarized radiation smear it out (Figures 3a and 4d).

For the forbidden photoionization (Figures 3d–f and 4a–c), general tendencies are quite different from the ones observed for the metastable states (Figures 1a–c and 2d–f). While there is no Cooper minimum in the photoionization of the metastable states and the cross-section drops down from the threshold, in the photoionization of the dipole-allowed states, the cross-section may increase from threshold (Figure 3d–f), indicating that the Cooper minimum has fallen under the threshold or appears above the threshold (Figure 4a–c). In the last case, the Cooper minimum is more pronounced for circularly polarized fields.

Calculations in the velocity gauge are again more sensitive to a model than in the length gauge and more sensitive when it comes to photoionization from $2s^2 2p^5 (^2P_{1/2}) 3s [1/2]_1$ than from $2s^2 2p^5 (^2P_{3/2}) 3s [3/2]_1$.

In comparison with the photoionization from the metastable states, the channels with $J = 0$ bring up two more autoionizing states: hole-particle $2s 2p^6 3s [^1S_0]$ AIS and doubly excited $2s^2 2p^4 3s^2 [^3P_0]$ AIS visible in case of linearly polarized and unpolarized light (Figures 3 and 4a,b,d,e). For unpolarized fields (Figures 3 and 4a,d), channels with $J = 1$ manifest resonance $2s 2p^6 3s [^3S_1]$, which dominates over the energy region. The parameters of the AISs are discussed in the next section.

4. The Resonance Structures

There are three lowest resonance structures of even parity: hole-particle resonances $2s 2p^6 3s (^{1,3}S_{0,1})$ generated on $2s 2p^6 (^2S_{1/2})$ target and doubly excited resonance $2s^2 2p^4 3s^2 (^3P_0)$ generated on $2s^2 2p^4 3s (^4P_{1/2})$ target. Within the jK-coupling scheme, the R-matrix [58] does not generate the AIS of configuration $2p^4 3s^2$ with $J = 1, 2$ on any of the target states $2p^4 3s (^4P_{3/2,5/2}, {}^2D_{3/2,5/2})$.

In Figure 5, there is the region with AISs excited from the metastable and dipole-allowed states by unpolarized fields plotted in a more detailed way for the models with six and ten targets. The AISs' positions are different due to interchannel interaction. The inclusion of $2s^2 2p^4 (^3P) 3s [^2D_J]$ lowers the position of the hole-particle resonances $2s 2p^6 3s [^{1,3}S_{0,1}]$ and, following the addition of higher targets, does not change them significantly. The inclusion of $2s^2 2p^4 (^3P) 3s [^2P_J]$ lowers the position of the doubly excited $2s^2 2p^4 (^3P) 3s^2 [^3P_0]$ resonance and places it in experimental position [64] in $\mathcal{C}$-model. The further inclusion of $2s^2 2p^4 (^3P) 3p [^4P_J]$ targets (not shown) does not improve the position of the doubly excited state: in the $\mathcal{C}$-model, it is pulled 0.3 eV below the experiment, while in the $\mathcal{V}$-model, it is by 0.6 eV above. It is found that the lowest AISs of even parity in neon are excited very effectively from the excited states and dominate over direct photoionization in the corresponding energy region.

The R-matrix approach does not produce values of energy E, width Γ and Fano profile index q [19], but one can fit a resonance structure and extract these values (see Table 2). All of the resonances are excited very efficiently, whereby transitions $2s \to 2p$ and $2p \to 3s$, as a result, the AISs are practically symmetric with huge q-indexes. The large value of q makes the extraction procedure problematic, and in Table 2, we replace $|q| > 100$ by ∞ with the corresponding sign. The particle-hole AISs' width ratio is close to the ratio of their statistical weights. The Fano index may take different values and signs depending on the state it is excited from, the target state and the polarization of radiation. The latter occurs because different contributions of the channels with different angular momentum J to the cross-sections result in different backgrounds and heights of resonance.

As for the doubly excited AIS $2p^4 3s^2 [^3P_J]$ within the jK-coupling scheme, there is only $2p^4 3s^2 [^3P_0]$ with $\Gamma \approx 0.003$ eV. Within the LSJ-coupling scheme, all of the triplet states $2p^4 3s^2 [^3P_J]$ are generated with $\Gamma \approx 0.001$ eV separated approximately by 0.15 eV. We checked that the hole-particle resonances are weakly affected by a coupling scheme and that they are just a little broadening ($\Gamma = 0.122$ and 0.079 eV). To the best of our knowledge,

there is no experiment able to resolve the fine structure of this AIS and the choice between the jK- and LSJ-coupling schemes for them is insurmountable so far.
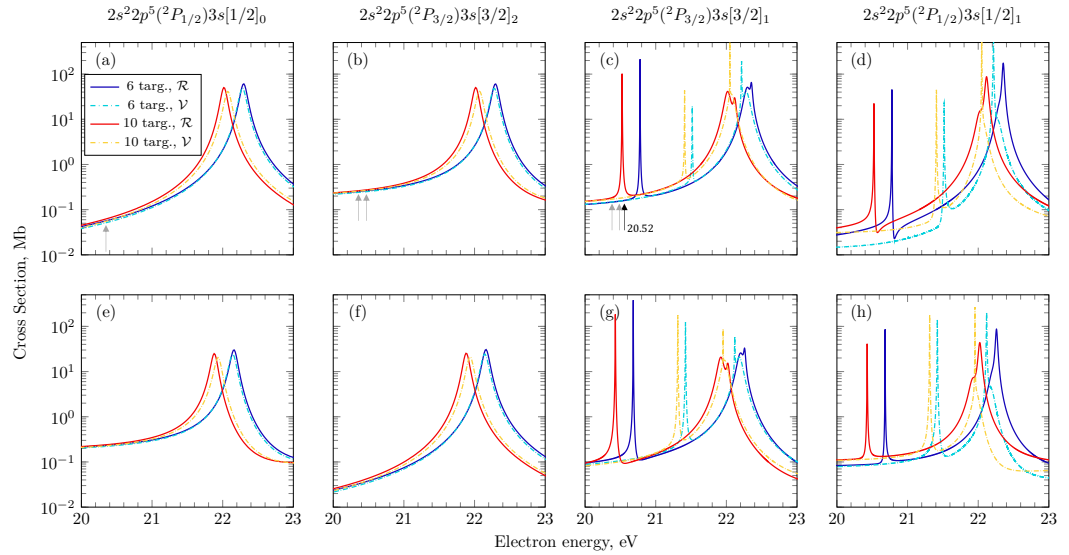

Figure 5. Cross-section calculated in the length gauge within the $\mathcal{V}$- (dash-dotted lines) and $\mathcal{C}$- (solid lines) models with six (cyan and blue) and ten (orange and red) thresholds for ionization of $2s^22p^5(^2P_{1/2})3s[1/2]_0$ (**a,e**), $2s^22p^5(^2P_{3/2})3s[3/2]_2$ (**b,f**) and $2s^22p^5(^2P_{3/2})3s[3/2]_1$ (**c,g**), $2s^22p^5(^2P_{1/2})3s[1/2]_1$ (**d,h**) states to $2s^22p^5(^2P_{3/2})$ (upper row) and to $2s^22p^5(^2P_{1/2})$ (bottom row) ionic states for unpolarized fields. The arrows mark positions of very narrow resonances $2p^43s^2[^2P_{J=1,2}]$ where they would appear within the LSJ-coupling scheme.

Table 2. AISs parameters in a model within ten target states: energy position E (eV), width Γ (eV) and Fano profile index q at excitation of different initial states for different polarization.

AIS / Parameter		$2s2p^63s\,[^3S_1]$	$2s2p^63s\,[^1S_0]$
E	$\mathcal{C}$-model	22.03	22.13
Γ		0.119	0.028
q^{un}	$(^2P_{3/2})3s[3/2]_1 \to 2p^5\,(^2P_{3/2})$	-70	∞
q^{un}	$(^2P_{3/2})3s[3/2]_1 \to 2p^5\,(^2P_{1/2})$	-50	-75
q^{un}	$(^2P_{1/2})3s[1/2]_1 \to 2p^5\,(^2P_{3/2})$	∞	∞
q^{un}	$(^2P_{1/2})3s[1/2]_1 \to 2p^5\,(^2P_{1/2})$	-15	∞
q^{lin}	$(^2P_{3/2})3s[3/2]_1 \to 2p^5\,(^2P_{3/2})$	-	∞
q^{lin}	$(^2P_{3/2})3s[3/2]_1 \to 2p^5\,(^2P_{1/2})$	-	-80
q^{lin}	$(^2P_{1/2})3s[1/2]_1 \to 2p^5\,(^2P_{3/2})$	-	$-\infty$
q^{lin}	$(^2P_{1/2})3s[1/2]_1 \to 2p^5\,(^2P_{1/2})$	-	∞
E	$\mathcal{V}$-model	22.07	22.05
Γ		0.116	0.002
q^{un}	$(^2P_{3/2})3s[3/2]_1 \to 2p^5\,(^2P_{3/2})$	-75	$-\infty$
q^{un}	$(^2P_{3/2})3s[3/2]_1 \to 2p^5\,(^2P_{1/2})$	-50	∞
q^{un}	$(^2P_{1/2})3s[1/2]_1 \to 2p^5\,(^2P_{3/2})$	65	∞
q^{un}	$(^2P_{1/2})3s[1/2]_1 \to 2p^5\,(^2P_{1/2})$	-15	∞
q^{lin}	$(^2P_{3/2})3s[3/2]_1 \to 2p^5\,(^2P_{3/2})$	-	$-\infty$
q^{lin}	$(^2P_{3/2})3s[3/2]_1 \to 2p^5\,(^2P_{1/2})$	-	∞
q^{lin}	$(^2P_{1/2})3s[1/2]_1 \to 2p^5\,(^2P_{3/2})$	-	$-\infty$
q^{lin}	$(^2P_{1/2})3s[1/2]_1 \to 2p^5\,(^2P_{1/2})$	-	$-\infty$

5. Conclusions

The photoionization cross-section of the lowest excited states of neon are presented. The R-matrix approach is applied with a variety of different parameters, and the comparison of the usability of real and virtual orbitals is carried out. Results are presented for the metastable states (total angular momentum $J = 0, 2$) ionized by unpolarized light and for the dipole-allowed states ($J = 1$) ionized by the light with the same polarization as those causing their excitation: unpolarized, linearly and circularly polarized. The spectroscopic features such as Cooper minimum, particle-hole and doubly excited autoionizing states are found to appear differently depending on polarization.

It was shown that the model based on virtual orbitals provides much better convergence in terms of length and velocity gauge, as well as in terms of target states involved. It predicts a deeper Cooper minimum placed at higher energy. On the other hand, $\mathcal{V}$-model has a tendency to become overcorrelated (unrealistically compact wave functions), which imposes the problem of a correct positioning of the narrow AISs. Based on real orbitals, the $\mathcal{C}$-model turns out to be more stable and better reproduces the AIS structures. The hole-particle AISs are found to be much broader than the doubly excited ones.

This work may serve as building blocks for the investigation of multi-photon, probably two-color ionization by VUV radiation.

Author Contributions: M.D.K. is responsible for the $\mathcal{V}$-model and M.M.P. for the $\mathcal{R}$-, $\mathcal{C}$-models. All of the authors took part in discussions of the results and preparing the manuscript. Conceptualization E.V.G. and A.N.G.-G.; investigation, formal analysis M.M.P. and M.D.K.; visualization M.M.P.; resources S.M.B.; writing—original draft preparation E.V.G., M.M.P. and M.D.K.; writing—review and editing M.M.P., M.D.K., S.M.B., E.V.G. and A.N.G.-G.; funding acquisition A.N.G.-G. and S.M.B. All authors have read and agreed to the published version of the manuscript.

Institutional Review Board Statement: Not applicable.

Informed Consent Statement: Not applicable.

Data Availability Statement: Not applicable.

Conflicts of Interest: The authors declare no conflict of interests.

References

1. Connerade, J. *Highly Exited Atoms*; Cambridge University Press: Cambridge, UK, 1998.
2. Baig, M.A. Measurement of Photoionization Cross-Section for the Excited States of Atoms: A Review. *Atoms* **2022**, *10*, 39. [CrossRef]
3. Avdonina, N.B.; Amusia, M.Y. Characteristic features in photoionisation of excited atomic states. *J. Phys. B At. Mol. Phys.* **1983**, *16*, L543–L545. [CrossRef]
4. Cooper, J.W. Interaction of Maxima in the Absorption of Soft X Rays. *Phys. Rev. Lett.* **1964**, *13*, 762–764. [CrossRef]
5. Fano, U.; Cooper, J.W. Spectral Distribution of Atomic Oscillator Strengths. *Rev. Mod. Phys.* **1968**, *40*, 441–507. [CrossRef]
6. Msezane, A.; Manson, S.T. New Minima in Photoionization Cross Section. *Phys. Rev. Lett.* **1975**, *35*, 364–366. [CrossRef]
7. Mamsom, S.T.; Cooper, J.W. Photo-Ionization in the Soft x-Ray Range: 1Z Dependence in a Central-Potential Model. *Phys. Rev.* **1968**, *165*, 126–138. [CrossRef]
8. McGuire, E.J. Photo-Ionization Cross Sections of the Elements Helium to Xenon. *Phys. Rev.* **1968**, *175*, 20–30. [CrossRef]
9. Amusia, M.; Chernysheva, L.; Yarzhemsky, V. *Handbook of Theoretical Atomic Physics: Data for Photon Absorption, Electron Scattering, and Vacancies Decay*; Springer Science & Business Media: Berlin/Heidelberg, Germany, 2012.

10. Amusia, M.; Kheifets, A. The influence of "two-electron-two-hole excitation"s on the $3s^{-1}4p$ autoionization profile in Ar atoms. *Phys. Lett. A* **1981**, *82*, 407–411. [CrossRef]

11. Amusia, M.Y.; Ivanov, V.K.; Cherepkov, N.A.; Chernysheva, L.V. Interference effects in photoionization of noble gas atoms outer s-shells. *Phys. Lett.* **1972**, *40A*, 361–362. [CrossRef]

12. Toffoli, D.; Stener, M.; Fronzoni, G.; Decleva, P. Convergence of the multicenter B-spline DFT approach for the continuum. *Chem. Phys.* **2002**, *276*, 25–43. [CrossRef]

13. Marante, C.; Klinker, M.; Corral, I.; González-Vázquez, J.; Argenti, L.; Martín, F. Hybrid-Basis Close-Coupling Interface to Quantum Chemistry Packages for the Treatment of Ionization Problems. *J. Chem. Theory Comput.* **2017**, *13*, 499–514. [CrossRef]

14. Moitra, T.; Ponzi, A.; Koch, H.; Coriani, S.; Decleva, P. Accurate Description of Photoionization Dynamical Parameters. *J. Phys. Chem. Lett.* **2020**, *11*, 5330–5337. [CrossRef]

15. Kheifets, A.S. Time delay in valence-shell photoionization of noble-gas atoms. *Phys. Rev. A* **2013**, *87*, 063404. [CrossRef]

16. Palatchi, C.; Dahlstrom, J.M.; Kheifets, A.S.; Ivanov, I.A.; Canaday, D.M.; Agostini, P.; DiMauro, L.F. Atomic delay in helium, neon, argon and krypton. *J. Phys. B At. Mol. Opt. Phys.* **2014**, *47*, 245003. [CrossRef]

17. Alexandridi, C.; Platzer, D.; Barreau, L.; Busto, D.; Zhong, S.; Turconi, M.; Neoričić, L.; Laurell, H.; Arnold, C.L.; Borot, A.; et al. Attosecond photoionization dynamics in the vicinity of the Cooper minima in argon. *Phys. Rev. Res.* **2021**, *3*, L012012. [CrossRef]

18. Saha, S.; Mandal, A.; Jose, J.; Varma, H.R.; Deshmukh, P.C.; Kheifets, A.S.; Dolmatov, V.K.; Manson, S.T. Relativistic effects in photoionization time delay near the Cooper minimum of noble-gas atoms. *Phys. Rev. A* **2014**, *90*, 053406. [CrossRef]

19. Fano, U. Effects of Configuration Interaction on Intensities and Phase Shifts. *Phys. Rev.* **1961**, *124*, 1866–1878. [CrossRef]

20. Arimondo, E.; Clark, C.W.; Martin, W.C. Colloquium: Ettore Majorana and the birth of autoionization. *Rev. Mod. Phys.* **2010**, *82*, 1947–1958. [CrossRef]

21. Madden, R.P.; Codling, K. New Autoionizing Atomic Energy Levels in He, Ne, and Ar. *Phys. Rev. Lett.* **1963**, *10*, 516–518. [CrossRef]

22. Baig, M.A.; Connerade, J.P. Centrifugal barrier effects in the high Rydberg states and autoionising resonances of neon. *J. Phys. B At. Mol. Phys.* **1984**, *17*, 1785–1796. [CrossRef]

23. Maeda, K.; Ueda, K.; Ito, K. High-resolution measurement for photoabsorption cross sections in the autoionization regions of Ar, Kr and Xe. *J. Phys. B At. Mol. Opt. Phys.* **1993**, *26*, 1541–1555. [CrossRef]

24. Kabachnik, N.M.; Sazhina, I.P. Angular distribution and polarization of photoelectrons in the region of resonances. *J. Phys. B At. Mol. Opt. Phys.* **1976**, *9*, 1681–1697. [CrossRef]

25. Pratt, S.T.; Dehmer, P.M.; Dehmer, J.L. Three-photon excitation of autoionizing states of atomic xenon between the $^{2\circ}{}_{3/2}$ and $^{2\circ}{}_{1/2}$ fine-structure thresholds. *Phys. Rev. A* **1987**, *35*, 3793–3798. [CrossRef]

26. Blazewicz, P.R.; Stockdale, J.A.D.; Miller, J.C.; Efthimiopoulos, T.; Fotakis, C. Four-photon excitation of even-parity Rydberg states in krypton and xenon. *Phys. Rev. A* **1987**, *35*, 1092–1098. [CrossRef]

27. Koeckhoven, S.M.; Buma, W.J.; de Lange, C.A. Three-photon excitation of autoionizing states of Ar, Kr, and Xe between the $^2P_{3/2}$ and $^2P_{1/2}$ ionic limits. *Phys. Rev. A* **1994**, *49*, 3322–3332. [CrossRef]

28. Moccia, R.; Rahman, N.K.; Rizzo, A. Two-photon ionisation cross section calculations of noble gases: Results for Ne and Ar. *J. Phys. B At. Mol. Opt. Phys.* **1983**, *16*, 2737–2751. [CrossRef]

29. Saenz, A.; Lambropoulos, P. Theoretical two-, three- and four-photon ionization cross sections of helium in the XUV range. *J. Phys. B At. Mol. Opt. Phys.* **1999**, *32*, 5629–5637. [CrossRef]

30. Aloïse, S.; O'Keeffe, P.; Cubaynes, D.; Meyer, M.; Grum-Grzhimailo, A.N. Photoionization of Synchrotron-Radiation-Excited Atoms: Separating Partial Cross Sections by Full Polarization Control. *Phys. Rev. Lett.* **2005**, *94*, 223002. [CrossRef]

31. Petrov, I.; Peters, T.; Halfmann, T.; Aloıse, S.; O'Keeffe, P.; Meyer, M.; Sukhorukov, V.; Hotop, H. Lineshapes of the even $mp^5_{1/2}5n(p'/f')$ autoionizing resonances of Ar, Kr and Xe. *Eur. Phys. J. D* **2006**, *40*, 181–193. [CrossRef]

32. O'Keeffe, P.; Bolognesi, P.; Mihelic, A.; Moise, A.; Richter, R.; Cautero, G.; Stebel, L.; Sergo, R.; Pravica, L.; Ovcharenko, E.; et al. Photoelectron angular distributions from polarized Ne* atoms near threshold. *Phys. Rev. A* **2010**, *82*, 052522. [CrossRef]

33. O'Keeffe, P.; Gryzlova, E.V.; Cubaynes, D.; Garcia, G.A.; Nahon, L.; Grum-Grzhimailo, A.N.; Meyer, M. Isotopically Resolved Photoelectron Imaging Unravels Complex Atomic Autoionization Dynamics by Two-Color Resonant Ionization. *Phys. Rev. Lett.* **2013**, *111*, 243002. [CrossRef] [PubMed]

34. Bartschat, K.; Madison, D.H. Electron impact excitation of rare gases: Differential cross sections and angular correlation parameters for neon, argon, krypton and xenon. *J. Phys. B At. Mol. Opt. Phys.* **1987**, *20*, 5839–5863. [CrossRef]

35. Knight, R.D.; guo Wang, L. One-photon laser spectroscopy of the np and nf Rydberg series in xenon. *J. Opt. Soc. Am. B* **1985**, *2*, 1084–1087. [CrossRef]

36. L'Huillier, A.; Lompré, L.A.; Normand, D.; Morellec, J.; Ferray, M.; Lavancier, J.; Mainfray, G.; Manus, C. Spectroscopy of the np and nf even-parity Rydberg series in xenon by two-photon excitation. *J. Opt. Soc. Am. B* **1989**, *6*, 1644–1647. [CrossRef]

37. McCann, K.J.; Flannery, M.R. Photoionization of metastable rare-gas atoms (He*,Ne*,Ar*,Kr*,Xe*). *Appl. Phys. Lett.* **1977**, *31*, 599–601. [CrossRef]

38. Kau, R.; Petrov, I.D.; Sukhorukov, V.L.; Hotop, H. Experimental and theoretical cross sections for photoionization of metastable atoms near threshold. *J. Phys. B At. Mol. Opt. Phys.* **1996**, *29*, 5673–5698. [CrossRef]

39. Kopeika, N.S.; Shuker, R.; Yerachmiel, Y.; Gabai, Y.; Ih, C.S. Observation of Cooper minima in excited-*s*-state photoionization cross sections in neon and argon. *Phys. Rev. A* **1983**, *28*, 1517–1526. [CrossRef]

40. Petrov, I.D.; Lagutin, B.M.; Sukhorukov, V.L.; Knie, A.; Ehresmann, A. Correlation and polarization effects in two-photon photoionization of Ar. *Phys. Rev. A* **2016**, *93*, 033408. [CrossRef]

41. Petrov, I.D.; Sukhorukov, V.L.; Hotop, H. Photoionization of excited Ne*$(2p^5 3p, J = 3)$ atoms near threshold. *J. Phys. B At. Mol. Opt. Phys.* **2008**, *41*, 065205. [CrossRef]

42. Sukhorukov, V.L.; Petrov, I.D.; Schafer, M.; Merkt, F.; Ruf, M.W.; Hotop, H. Photoionization dynamics of excited Ne, Ar, Kr and Xe atoms near threshold. *J. Phys. B At. Mol. Opt. Phys.* **2012**, *45*, 092001. [CrossRef]

43. Gallagher, T.F. Quantum defect theory. In *Rydberg Atoms*; Cambridge Monographs on Atomic, Molecular and Chemical Physics; Cambridge University Press: Cambridge, UK, 1994; pp. 415–428. [CrossRef]

44. Ojha, P.C.; Burke, P.G. Photoionisation of the $3p^5 4s$ excited states of argon. *J. Phys. B At. Mol. Opt. Phys.* **1983**, *16*, 3513–3529. [CrossRef]

45. Petrov, I.D.; Sukhorukov, V.L.; Hollenstein, U.; Kaufmann, L.J.; Merkt, F.; Hotop, H. Autoionization dynamics of even Ar $(3p^5_{1/2}np', nf')$ resonances: Comparison of experiment and theory. *J. Phys. B At. Mol. Opt. Phys.* **2011**, *44*, 025004. [CrossRef]

46. Gryzlova, E.V.; O'Keeffe, P.; Cubaynes, D.; Garcia, G.A.; Nahon, L.; Grum-Grzhimailo, A.N.; Meyer, M. Isotope effects in resonant two-color photoionization of Xe in the region of the $5p^5(^2P_{1/2})4f[5/2]_2$ autoionizing state. *N. J. Phys.* **2015**, *17*, 043054. [CrossRef]

47. McKenna, C.; van der Hart, H.W. Multiphoton ionization cross sections of neon and argon. *J. Phys. B At. Mol. Opt. Phys.* **2003**, *37*, 457–470. [CrossRef]

48. van der Hart, H.W.; Greene, C.H. Multichannel photoionization spectroscopy of Ar: Total cross section and threshold photoelectrons. *Phys. Rev. A* **1998**, *58*, 2097–2105. [CrossRef]

49. Hamonou, L.; Lysaght, M.A.; van der Hart, H.W. Influence of autoionizing states on the pulse-length dependence of strong-field Ne$^+$ photoionization at 38.4 eV. *J. Phys. B At. Mol. Opt. Phys.* **2010**, *43*, 045601. [CrossRef]

50. Zhou, Z.; Chu, S.I. Time-dependent localized Hartree-Fock density-functional linear response approach for photoionization of atomic excited states. *Phys. Rev. A* **2009**, *79*, 053412. [CrossRef]

51. Edwards, A.K.; Rudd, M.E. Excitation of Auto-Ionizing Levels in Neon by Ion Impact. *Phys. Rev.* **1968**, *170*, 140–144. [CrossRef]

52. Olsen, J.O.; Anderson, N. Autoionizing levels in neon excited by low-energy heavy-ion impact. *J. Phys. B At. Mol. Opt. Phys.* **1977**, *10*, 101–110. [CrossRef]

53. Jureta, J.J.; Marinković, B.P.; Milosavljević, A.R.; Avaldi, L. Singly and doubly excited states in ejected electron spectra of neon at high incident electron energies. *Eur. Phys. J. D* **2015**, *69*, 74. [CrossRef]

54. Prince, K.C.; Allaria, E.; Callegari, C.; Cucini, R.; Ninno, G.D.; Mitri, S.D.; Diviacco, B.; Ferrari, E.; Finetti, P.; Gauthier, D.; et al. Coherent control with a short-wavelength free-electron laser. *Nat. Photonics* **2016**, *10*, 176. [CrossRef]

55. You, D.; Ueda, K.; Gryzlova, E.V.; Grum-Grzhimailo, A.N.; Popova, M.M.; Staroselskaya, E.I.; Tugs, O.; Orimo, Y.; Sato, T.; Ishikawa, K.L.; et al. New Method for Measuring Angle-Resolved Phases in Photoemission. *Phys. Rev. X* **2020**, *10*, 031070. [CrossRef]

56. Gryzlova, E.V.; Carpeggiani, P.; Popova, M.M.; Kiselev, M.D.; Douguet, N.; Reduzzi, M.; Negro, M.; Comby, A.; Ahmadi, H.; Wanie1, V.; et al. Influence of an atomic resonance on the coherent control of the photoionization process. *Phys. Rev. Res.* **2022**, *4*, 033231. [CrossRef]

57. Gryzlova, E.V.; Ma, R.; Fukuzawa, H.; Motomura, K.; Yamada, A.; Ueda, K.; Grum-Grzhimailo, A.N.; Kabachnik, N.M.; Strakhova, S.I.; Rouzée, A.; et al. Doubly resonant three-photon double ionization of Ar atoms induced by an EUV free-electron laser. *Phys. Rev. A* **2011**, *84*, 063405. [CrossRef]

58. Zatsarinny, O. BSR: B-spline atomic R-matrix codes. *Comput. Phys. Commun.* **2006**, *174*, 273–356. [CrossRef]

59. Fischer, C.F. Towards B-Spline Atomic Structure Calculations. *Atoms* **2021**, *9*, 50. [CrossRef]

60. Zatsarinny, O.; Bartschat, K. B-spline calculations of oscillator strengths in noble gases. *Phys. Scr.* **2009**, *T134*, 014020. [CrossRef]

61. Zatsarinny, O.; Tayal, S.S. Photoionization of potassium atoms from the ground and excited states. *Phys. Rev. A* **2010**, *81*, 043423. [CrossRef]

62. Fischer, C.F.; Brage, T.; Johnsson, P. *Computational Atomic Structure. An MCHF Approach*; IOP Publishing: Bristol, UK, 1997.

63. Zatsarinny, O.; Fischer, C.F. A general program for computing angular integrals of the Breit–Pauli Hamiltonian with non-orthogonal orbitals. *Comput. Phys. Commun.* **2000**, *124*, 247–289. [CrossRef]

64. Wilden, D.G.; Hicks, P.J.; Comer, J. Electron impact studies of resonances and autoionizing states of neon. *J. Phys. B At. Mol. Phys.* **1977**, *10*, 1477–1486. [CrossRef]

65. *NIST Atomic Spectra Database (Version 5.8)*; National Institute of Standards and Technology: Gaithersburg, MD, USA, 2020. Available online: https://physics.nist.gov/asd (accessed on 18 May 2020).

66. Zeman, V.; Bartschat, K. Electron-impact excitation of the and states of neon. *J. Phys. B At. Mol. Opt. Phys.* **1997**, *30*, 4609–4622. [CrossRef]

67. Khakoo, M.A.; Wrkich, J.; Larsen, M.; Kleiban, G.; Kanik, I.; Trajmar, S.; Brunger, M.J.; Teubner, P.J.O.; Crowe, A.; Fontes, C.J.; et al. Differential cross sections and cross-section ratios for the electron-impact excitation of the neon $2p^5 3s$ configuration. *Phys. Rev. A* **2002**, *65*, 062711. [CrossRef]

68. Kheifets, A. Revealing the Target Electronic Structure with Under-Threshold RABBITT. *Atoms* **2021**, *9*, 66. [CrossRef]

69. Baier, S.; Grum-Grzhimailo, A.N.; Kabachnik, N.M. Angular distribution of photoelectrons in resonant photoionization of polarized atoms. *J. Phys. B At. Mol. Opt. Phys.* **1994**, *27*, 3363–3388. [CrossRef]